

A spatial correlation analysis for a toroidal universe

Ralf Aurich¹

¹Institut für Theoretische Physik, Universität Ulm,
Albert-Einstein-Allee 11, D-89069 Ulm, Germany

Abstract. The spatial cross-correlation function ξ_C recently introduced by Roukema et al. [1] is applied to an equilateral toroidal topology of the universe. Several CMB maps based on the WMAP 3yr and 5yr data are analysed and a small likelihood in favour of a torus cell is revealed. The results are compared to five Λ CDM simulations which point to a high false positive rate of the spatial-correlation-function method such that a firm conclusion cannot be drawn.

PACS numbers: 98.80.-k, 98.70.Vc, 98.80.Es

1. Introduction

The cosmic microwave background radiation (CMB) provides not only the information to constrain the cosmological parameters, but also has the potential to reveal the global structure of the Universe, i. e. its topology [2, 3, 4]. One method to reveal the topology is the search for the so-called circles-in-the-sky signature [5]. The CMB descends from the surface of last scattering (SLS) which is the spherical surface around an observer at which matter recombines. In the case of a multiply connected universe this sphere intersects with its “copies” due to the group of deck transformations defining the topology. Since the intersection of two spheres is a circle, one obtains pairs of circles along which the temperature fluctuations are identical, or at least, if we could receive the CMB as a pure signal proportional to the gravitational field on the SLS. Modifications due to the Doppler and the integrated Sachs-Wolfe effect are different on two paired circles thus preventing identical temperature fluctuations along paired circles. A further complication arises from the uncertainties of foreground emissions which additionally influence the observed CMB. Applications of the circles-in-the-sky signature to the WMAP data [6, 7] can be found in [8, 9, 10, 11, 12].

The circles-in-the-sky method has the disadvantage that it utilizes only the one-dimensional pixel information along paired circles. To circumvent this problem it is proposed in [1] that instead of analyzing correlations along the circles, one should define two *spatial* correlation functions ξ_A and ξ_C which also depend on pixels not lying on paired circles. The comparison of ξ_A with ξ_C provides then the topological signature. The idea is the following. The topology is defined by the group of deck transformations Γ , i. e. a discrete subgroup of isometries without fixed points. All spatial

points $q_1, q_2 \in \mathcal{M}^{(3)}$ obeying $q_1 = \gamma(q_2)$ for $\gamma \in \Gamma$ are identified, i. e. the spatial comoving space section $\mathcal{M}^{(3)}$ is tessellated by considering the quotient $\mathcal{M}^{(3)}/\Gamma$. Define now the set $\tilde{\Gamma}$ which contains the elements of Γ but the identity removed. With respect to this $\tilde{\Gamma}$ the distance d_{topo} between two points $q_1, q_2 \in \mathcal{M}^{(3)}$ is defined as

$$d_{\text{topo}}(q_1, q_2) := \min_{\gamma \in \tilde{\Gamma}} d(q_1, \gamma(q_2)) \quad , \quad (1)$$

where $d(q, q')$ is the usual spatial comoving distance in the universal covering space $\mathcal{M}^{(3)}$. Note, that for sufficiently nearby points q_1 and q_2 one has $d_{\text{topo}}(q_1, q_2) > d(q_1, q_2)$ since the identity is not contained in $\tilde{\Gamma}$. The reverse applies for sufficiently far separated points q_1 and q_2 . Now the two spatial correlation functions ξ_A and ξ_C can be defined as

$$\xi_A(r) := \langle \delta T(q_1) \delta T(q_2) \rangle \quad \text{with} \quad r = d(q_1, q_2) \quad (2)$$

for the auto-correlation function and

$$\xi_C(r) := \langle \delta T(q_1) \delta T(q_2) \rangle \quad \text{with} \quad r = d_{\text{topo}}(q_1, q_2) \quad (3)$$

for the cross-correlation function. Here, $\delta T(q)$ denotes the temperature fluctuation of the CMB in the direction \hat{n} corresponding to q and $\langle \dots \rangle$ the averaging over the pixels with $r = d(q_1, q_2)$ or $r = d_{\text{topo}}(q_1, q_2)$. In the practical analysis a binning with respect to r is necessary due to the pixelized sky maps.

The auto-correlation function $\xi_A(r)$ is the usual spatial correlation function which has a pronounced peak at $r = 0$. In the cross-correlation function $\xi_C(r)$ this peak has to be produced by points far separated on the sky which are topologically adjacent due to d_{topo} . One has detected the correct group Γ when both correlation functions $\xi_A(r)$ and $\xi_C(r)$ are identical, if it were not for the same modifications of the CMB which also plague the circles-in-the-sky method. The main advantage over the circles-in-the-sky method is that the correlations ξ_A and ξ_C are computed from a much larger set of pixels which levels out the modifications to some degree. On the other hand, since the spatial quantities ξ_A and ξ_C are three-dimensional measures which are only sampled from the two-dimensional SLS, one cannot expect ξ_A and ξ_C to be identical for statistical reasons.

To illustrate the difference between the two methods Fig. 1 displays the distance

$$d_{\min}(q) := \min_{q'} d_{\text{topo}}(q, q') \quad (4)$$

for the toroidal topology where all three side lengths are equal to $L = 4$ (in units of the Hubble length $L_H = c/H_0$, see section 2) and the symmetry axis pointing to the north pole. The number of pixels used to discriminate the topology for a given orientation is much larger for the spatial-correlation-function method than for the circles-in-the-sky method which utilizes only the pixels along the circles with $d_{\min} = 0$. In this work all pixels inside the kp0 mask [6] are excluded which are contaminated by the milky way and other foreground sources. These excluded domains are shown in black in Fig. 1.

The spatial-correlation-function method works best if there is a large number of pixel pairs with small topological distances d_{topo} , since the peak of the correlation function at $r = 0$ can then be tested with a good statistical significance. In units of

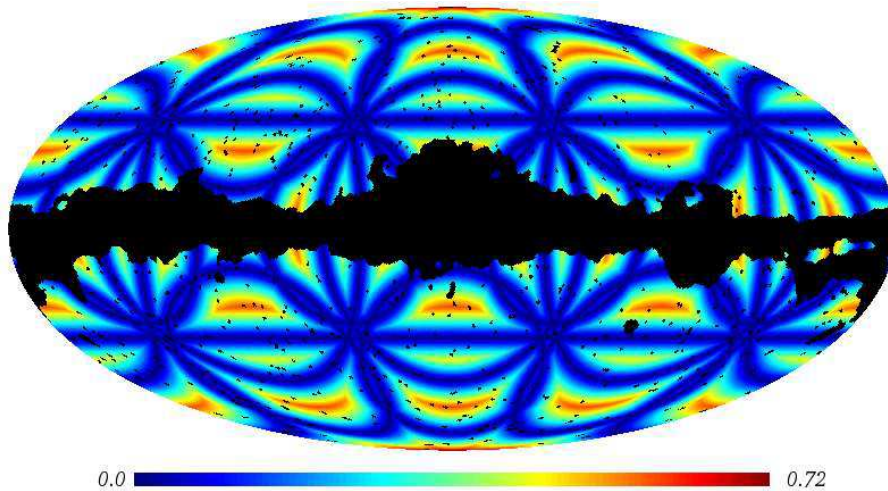


Figure 1. The distance $d_{\min}(q)$, eq. (4), is shown for the equilateral toroidal universe with side length $L = 4$ in the Mollweide projection. The paired circles correspond to $d_{\min} = 0$, i.e. the dark blue regions. The black regions show the pixels excluded by the kp0 mask used throughout this paper.

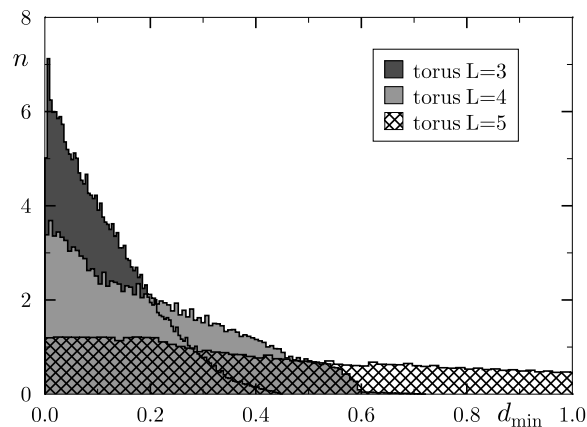


Figure 2. The distribution of the number of pixel pairs in dependence on d_{\min} is shown for three different sizes of the toroidal cell. For the model with side length $L = 3, 4$ and 5 all points on the SLS have a largest distance d_{\min} of $0.45, 0.72$ and 1.66 , respectively. With decreasing torus size the number of pixel pairs with $d_{\min} < 0.2$ increases significantly.

the Hubble length one needs the correlation functions for $r < 1$. For this reason Fig. 2 presents the distribution of the number of pixel pairs with respect to d_{\min} for three different sizes of the toroidal fundamental cell. A large number of pixel pairs close to $d_{\min} = 0$ is observed only for sufficiently small tori. Since d_{\min} is the lower bound of the distance for which the data are sampled for the estimation of the correlation functions, this implies that with increasing L the statistical significance for the estimates of $\xi_C(r)$ for small values of r diminishes. Thus for too large fundamental cells the spatial-correlation-function method has the same problems as the circles-in-the-sky method. In the latter case the number and the sizes of paired circles declines with increasing side length L until there are none at all. In the following the analysis is restricted to $L < 5$.

In Roukema et al. [1] the spatial-correlation-function method is applied to the Poincaré dodecahedron and a special orientation is found for which an enhanced likelihood occurs. In this paper, the flat toroidal topology with the additional restriction that all side lengths are equal is in the focus in order to see how this topology behaves using the method of [1].

2. The Markov Chain Monte Carlo method for the toroidal universe

The toroidal topology is defined on the universal covering space $\mathcal{M}^{(3)} = \mathbb{R}^3$ on which the points $q = (x, y, z) \in \mathbb{R}^3$ and $q' = (x', y', z') \in \mathbb{R}^3$ are identified for

$$q' = (x + n_x L_x, y + n_y L_y, z + n_z L_z) \quad \text{with} \quad (n_x, n_y, n_z) \in \mathbb{Z}^3 \quad . \quad (5)$$

Since the group Γ is infinite, a finite subset of $\tilde{\Gamma}$ has to be chosen for the computation of the distance $d_{\text{topo}}(q_1, q_2)$ in eq. (1). Here, the subset is restricted to the group elements which lead to copies of the fundamental cell directly adjacent over a face, an edge or a corner, i.e. to the elements with $|n_x| \leq 1$, $|n_y| \leq 1$, $|n_z| \leq 1$ and excluding $(n_x, n_y, n_z) = (0, 0, 0)$, of course. The minimum in eq. (1) is thus determined over 26 group elements. As already stated, only an equilateral toroidal cell is considered in the following, i.e. $L = L_x = L_y = L_z$. The lengths L are given in units of the Hubble length $L_H = c/H_0$. For the conversion of the CMB correlation to the spatial correlation, the distance to the SLS is required, which in turn is determined by the chosen cosmological parameters. For the Λ CDM model one gets from Table 2 in [13] the cosmological parameters based on all astronomical observations, see their column “3 Year + ALL Mean”, i.e. $\Omega_b = 0.044$, $\Omega_{\text{cdm}} = 0.223$, $\Omega_\Lambda = 0.733$, $h = 0.704$, $n_s = 0.947$, $\tau = 0.073$. For these values the distance to the SLS is $L_{\text{SLS}} = \Delta\eta L_H \simeq 14.2 \text{ Gpc}$ where $\Delta\eta = \eta_0 - \eta_{\text{SLS}} = 3.329$ (η is the conformal time).

As in [1] the Markov Chain Monte Carlo (MCMC) method with the Metropolis algorithm [14] is used in order to determine the most likely side length L together with the orientation of the fundamental cell defined by the three Euler angles (α, β, γ) . This leads to a four parameter $(L, \alpha, \beta, \gamma)$ search. The Metropolis algorithm requires the specification of a probability estimator P which determines the probability $\min(1, P_{\text{new}}/P_{\text{old}})$ with which a new state is accepted in the Markov chain. In [1] this probability is chosen as

$$P := \prod_{i=1}^n \begin{cases} e^{-\frac{|\xi_C(i) - \xi_A(i)|^2}{2\sigma_i^2}} & \text{for } \xi_C(i) \leq \xi_A(i) \\ 1 + 0.01 \frac{\xi_C(i) - \xi_A(i)}{\xi_A(i)} & \text{for } \xi_C(i) \geq \xi_A(i) \end{cases} \quad , \quad (6)$$

with

$$\sigma_i := \frac{1}{2} \xi_A(i) \sqrt{\frac{N_n}{N_i}} \quad . \quad (7)$$

Here, the index i runs over the bins for which the values of ξ_C and ξ_A are sampled and N_i denotes the number of pixel pairs contributing to bin i . See ref. [1] for details and a

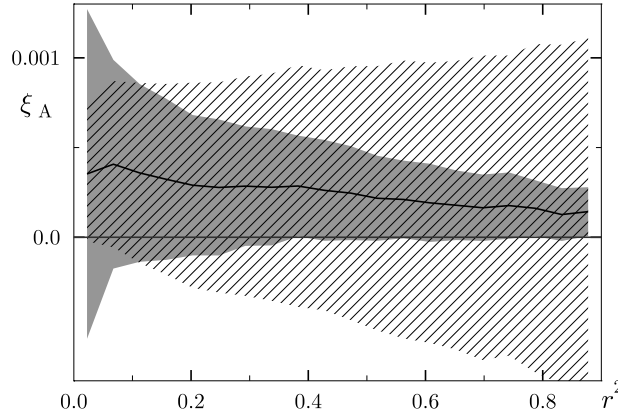


Figure 3. The different behaviour of the σ , eq. (7), and $\hat{\sigma}$, eq. (8), is illustrated. The grey region shows $\xi_A \pm \sigma$ which increases with decreasing distances r . The reverse behaviour is displayed by $\xi_A \pm \hat{\sigma}$ shown as the hatched area.

discussion motivating this choice. Since σ_i is larger for bins having fewer entries N_i , the probability P weights the bins according to their statistical significance. The smaller the distance d_{topo} is, the smaller is also the number of pixel pairs contributing to the corresponding bin. However, it is just the behaviour at small distances, i. e. the peak at $r = 0$ in $\xi_A(r)$, which has to be reproduced by $\xi_C(r)$ if the supposed group Γ matches the true one. For this reason a second probability \hat{P} is used in this paper, which emphasizes the peak at $r = 0$ by using instead of the above σ_i , eq. (7), the following alternative

$$\hat{\sigma}_i := \bar{\xi}_A \sqrt{\frac{\bar{\xi}_A}{\xi_A(i)}} \quad \text{with} \quad \bar{\xi}_A := \frac{1}{n} \sum_{i=1}^n \xi_A(i) \quad . \quad (8)$$

For large values of $\xi_A(i)$ a small $\hat{\sigma}_i$ is obtained thus selecting models producing strong correlations at $r = 0$. This probability is complementary to the former one. It, however, ignores the number of entries on which the value of the bin i is based.

Since the number of entries into a bin increases linearly for an equidistant binning in r for $\xi_A(i)$, an equidistant binning with respect to r^2 is used in this paper. This leads to N_i of the same order. For such a binning the complementary behaviour of σ and $\hat{\sigma}$ is shown in Fig. 3. The sky maps are in the HEALPix format [15] and are analysed for $n_{\text{side}} = 128$. Since these maps have $12n_{\text{side}}^2$ pixels, only every 10th pixel is actually used in order to keep the numerical effort manageable. Without using a mask this leads to $N_{\text{pix}} = 19661$ pixels, and using the kp0 mask which cuts out 23% of the area, $N_{\text{pix}} = 15052$ pixels contribute to the computation of ξ_A and ξ_C . In the likelihood (6) $n = 20$ equidistant bins are used from $r^2 = 0$ to $r^2 = 0.9$.

A MCMC run is started by generating an initial point $(L_i, \alpha_i, \beta_i, \gamma_i)$ of the parameter space with an equidistributed random number generator. The initial values of L_i are from the interval $L_i \in [3.25, 4.75]$. By using the Metropolis algorithm, the Markov chain is not restricted to this interval, however. The initial Euler angles are equidistributedly chosen from the interval $[-\frac{\pi}{2}, \frac{\pi}{2}]$. Because of the symmetry of the toroidal fundamental cell there is some redundancy in the sense that the set of Euler angles does not uniquely

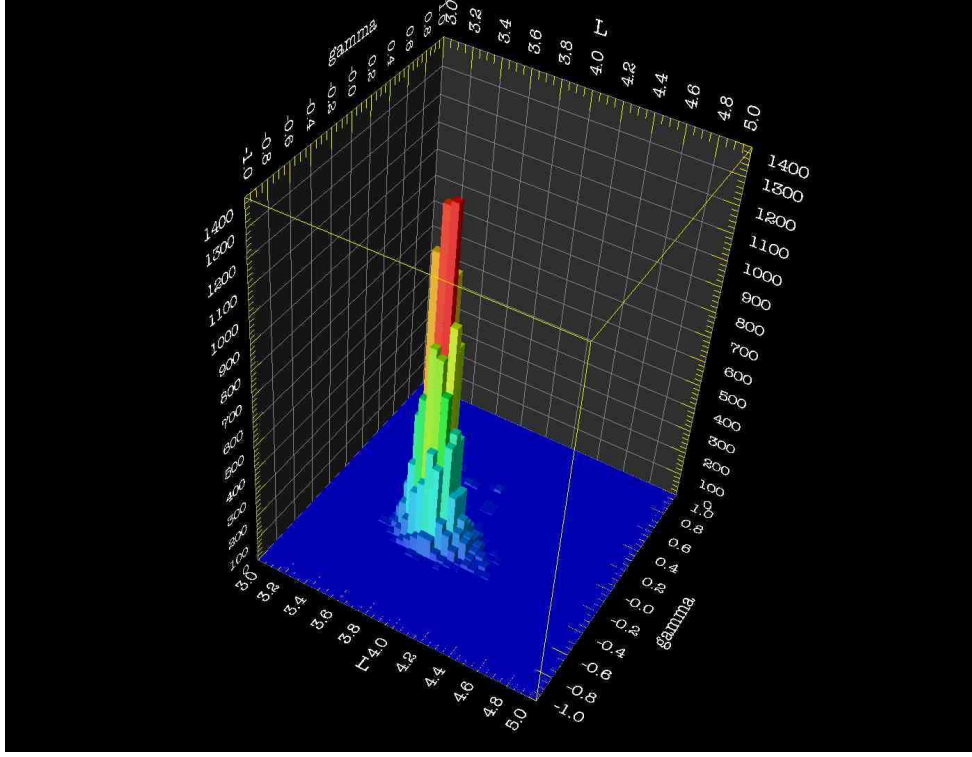


Figure 4. The distribution of the states of a Markov chain obtained from the ILC 5yr map with the kp0 mask is shown in dependence on the length L and the Euler angle γ . The likelihood function with σ , eq. (7), has been used.

define the orientation, i. e. several sets of Euler angles can give the same values for the Galactic coordinates of the symmetry axes of the fundamental cell. In the following the symmetry axes denote the directions in which one arrives at the centre of the nearest copies of the torus cell by a shift of length L , i. e. the face-to-face neighbours.

3. The spatial-correlation-function signature for the toroidal universe

Applying the MCMC method described in section 2 to the toroidal topology one observes that, after the initial “burn in”, most Markov chains occupy a region in the parameter space corresponding to a side length $L \simeq 3.8$ using the WMAP-ILC map based on the 5yr data [7] outside the kp0 mask. Fig. 4 shows the distribution of a Markov chain with respect to the two parameters L and γ ignoring α and β . The distribution is localized around a small region in parameter space with Euler angles corresponding to the Galactical coordinates of the toroidal symmetry axes given in Tab. 1. However, this nice behaviour is not observed for all Markov chains. If the initial length L_i is too large, i. e. near 4.75, the Markov chains drift towards increasing values of L . This is due to the decreasing statistical significance with increasing size of the fundamental cell. As shown in Fig. 2 the number of pixels $N_r := \#\{q | d_{\min}(q) < r\}$ which give information about the small distance behaviour of the cross-correlation function $\xi_C(r)$, decreases

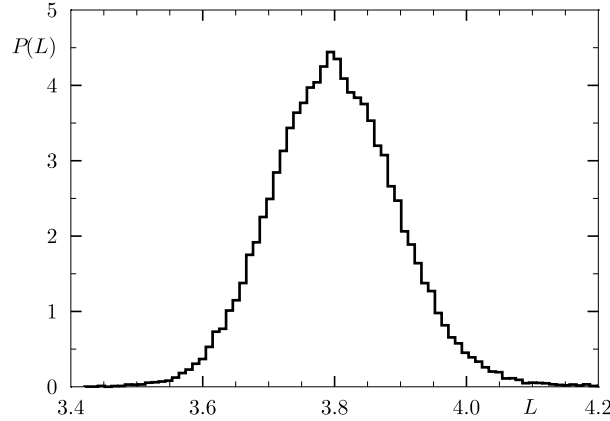


Figure 5. The normalized distribution of the states of several Markov chains obtained from the ILC 5yr map with the kp0 mask is shown in dependence on the length L . The likelihood function with σ , eq. (7), has been used. The states of several chains are merged so that the shown histogram is based on 150 000 states. These chains lead to $L = 3.80 \pm 0.09$.

l	12°	96°	174°	192°	276°	354°
b	-34°	9°	-56°	34°	-9°	56°

Table 1. The mean values of the orientation of the torus in Galactic coordinates (l, b) obtained from the five Markov chains shown in Fig. 5. The accuracy is of order 2° .

with increasing value of L . Thus, the probability that the few remaining pixels generate by chance a peak at $r = 0$ in $\xi_C(r)$ rises with increased values of L . This unsatisfactory behaviour might be remedied by choosing another probability function as (6). This topic will be addressed in a future study.

After having found a preferred region around $L = 3.8$, ten MCMC runs are carried out which use initial values $(L_i, \alpha_i, \beta_i, \gamma_i)$ within the likely domain. These ten chains provide 150 000 states from which the torus orientation and the torus size L is estimated. Fig. 5 shows the distribution of L for these Markov chains. An estimate of $L = 3.80 \pm 0.09$ is obtained. The directions of the corresponding symmetry axes, i.e. the directions to the six centres of the nearest face-to-face neighbours, are shown in Fig. 6 in Galactic coordinates using the same Mollweide projection as in Fig. 1. The image displays a preferred orientation, whose coordinates are given in Tab. 1. A second slightly shifted though less pronounced orientation is visible in Fig. 6 in pale blue.

The topological mirror image of our galaxy cluster is beyond the SLS because the topological scale $L \simeq 3.8$ is greater than the distance $\Delta\eta = 3.329$ to the SLS assuming the cosmological parameters stated in section 2. The nearest mirror images of objects at the centres of the “faces” of the torus, however, occur at half that length $L/2 \simeq 1.9$ from our point of view corresponding to a redshift $z \simeq 5.1$, i.e. there should be the same objects at the antipodal points of Tab. 1 at this redshift. The strong dependence of this redshift on the distance $L/2$ is shown in Fig. 7.

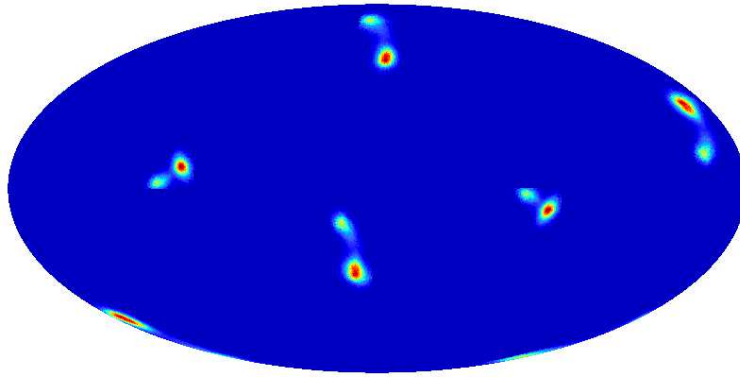


Figure 6. The orientations of the symmetry axes of the Markov chains used in Fig. 5 are shown on the sky in the Mollweide projection.

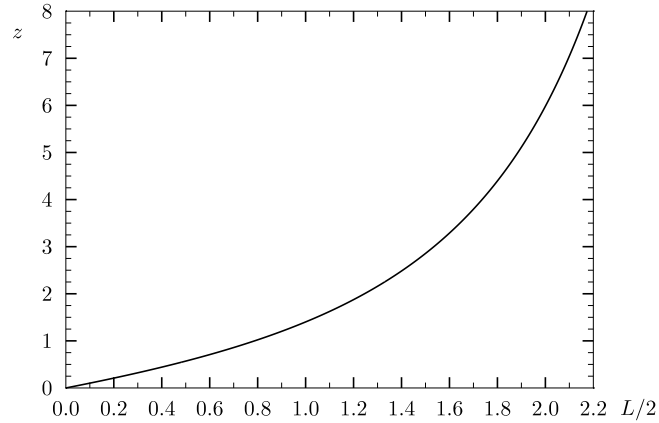


Figure 7. The redshift z at which antipodal objects occur in the direction of the nearest face-to-face neighbours is shown in dependence on the distance $L/2$ using the cosmological parameters stated in section 2.

In order to test whether the spatial-correlation-function signature is also present in the sky maps of a single frequency band, five MCMC runs are applied to each of the three bands Q, V and W. For these three bands, foreground reduced maps are available from the WMAP team [6] based on the three year data. Here the alternative probability function which is based on $\hat{\sigma}$, eq. (8), is used. It turns out that the Q band has difficulties to reveal the torus cell with $L \simeq 3.8$. In Fig. 8 the distribution of the states of one of the MCMC runs is shown. Although the peak close to $L \simeq 3.8$ is present, there are also other maxima such that the signature does not clearly point to a single maximum. This band is contaminated mainly by synchrotron and free-free emission. A possible explanation for the multi-peak structure in Fig. 8 might be that there are remaining foreground emissions which degrade the signature. In contrast, the V band, where the synchrotron and free-free emission is less important, displays a single peak as shown in Fig. 9. Although the peak is somewhat less pronounced in the foreground reduced W band which is mainly contaminated by dust emission, it is clear enough to reveal a single peak. Thus the spatial-correlation-function signature is most clearly seen in the

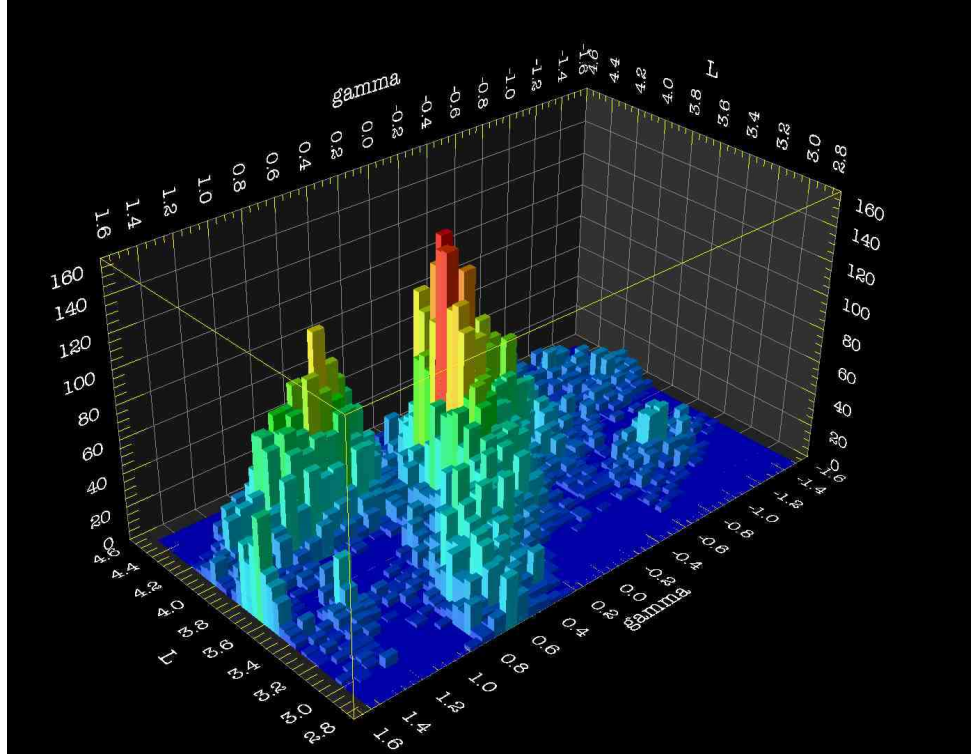


Figure 8. The distribution of the states of a Markov chain obtained from the foreground reduced Q band 3yr map with the kp0 mask is shown in dependence on the length L and the Euler angle γ . The likelihood function with $\hat{\sigma}$, eq. (8), has been used.

V band, followed by the W band, and only marginally present in the Q band.

It is worthwhile to remark that the results do not depend on the chosen probability function, i.e. using σ or $\hat{\sigma}$ in (6). Thus the algorithm is robust with respect to these two probabilities. Furthermore, the convergence of the Markov chains is checked by computing the MCMC power spectrum and the convergence ratio r along the lines described in [16].

4. Discussion

Does the analysis of the preceding section indeed point to a toroidal topology of the Universe or is the enhanced likelihood around $L \simeq 3.8$ a statistical fluke? It could be possible that the different contributions to the CMB, i.e. mainly the usual Sachs-Wolfe contribution, the Doppler effect, and the integrated Sachs-Wolfe contribution conspire in such a way that the cross-correlation function $\xi_C(r)$ gets by chance relative large values at small distances for the obtained orientation and torus size.

In order to settle this question one has to generate a large number of Λ CDM random sky simulations with the cosmological parameters of the standard model and apply the algorithm to them. This would yield the probability by which such a spatial-correlation-function signature would give a false positive. However, the numerical effort for such an

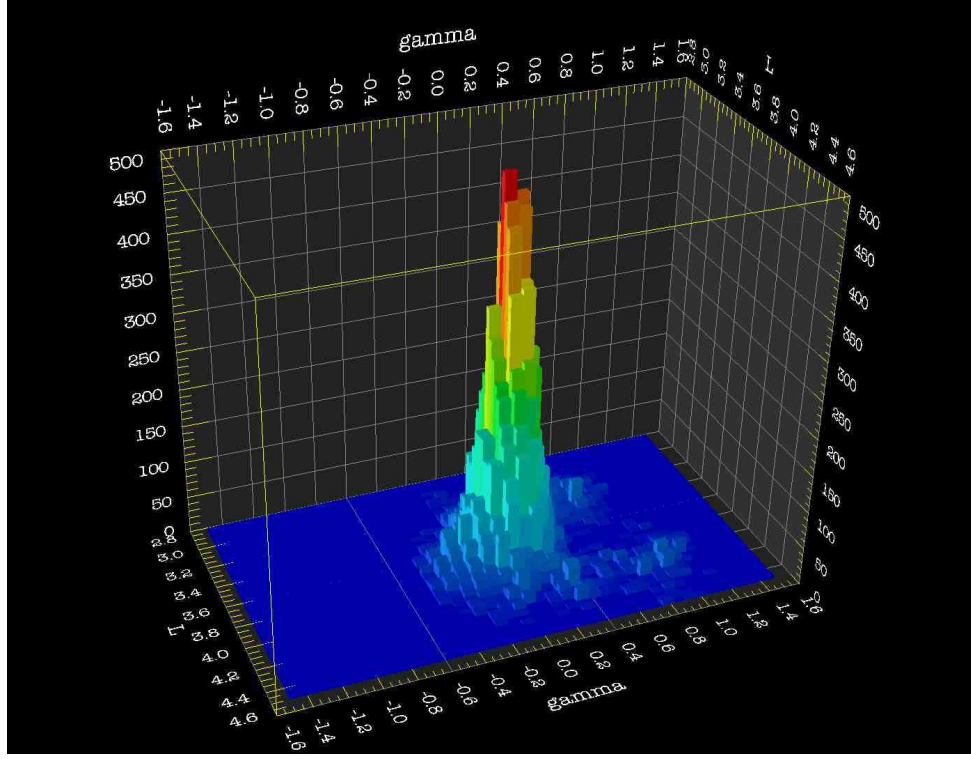


Figure 9. The distribution of the states of a Markov chain obtained from the foreground reduced V band 3yr map with the kp0 mask is shown in dependence on the length L and the Euler angle γ . The likelihood function with $\hat{\sigma}$, eq.(8), has been used.

investigation is prohibitive. Thus, only five Λ CDM sky maps are generated here using the cosmological parameters stated in section 2. For each of the five sky maps, five MCMC runs are carried out and analyzed. For all sky maps the kp0 mask is applied. No maxima at small values of L are found for four out of the five simulations. In these cases the Markov chains are found drifting to ever larger values of L which means, as discussed above, a decreasing significance for a detection. However, one of the five models produces such a nice peak structure as seen in Figs. 4 and 9 but around $L \simeq 4.1$. The corresponding cross-correlation ξ_C matches the auto-correlation ξ_A even better than in the best match for the torus using the real data as shown in Fig. 10. Based on this limited observation one might conclude that $\sim 20\%$ of the simulations would produce such a false positive detection. This is a very high level and thus, the conclusion should rather be that, if the topology is an equilateral toroidal one, then the torus has probably the side length $L \simeq 3.8$ and the orientation given in Tab. 1.

It is intriguing that the two-point temperature correlation function $C(\vartheta) := \langle \delta T(\hat{n}) \delta T(\hat{n}') \rangle$, $\hat{n} \cdot \hat{n}' = \cos \vartheta$, also suggests a torus size around $L \simeq 3.86$ when analyzed with the 3yr ILC map and applying the kp0 mask [17]. Evaluating $C(\vartheta)$ without applying the kp0 mask leads, however, to $L \simeq 4.35$. But nevertheless, both the observed low power at large scales in the CMB sky map as well as the spatial-correlation-

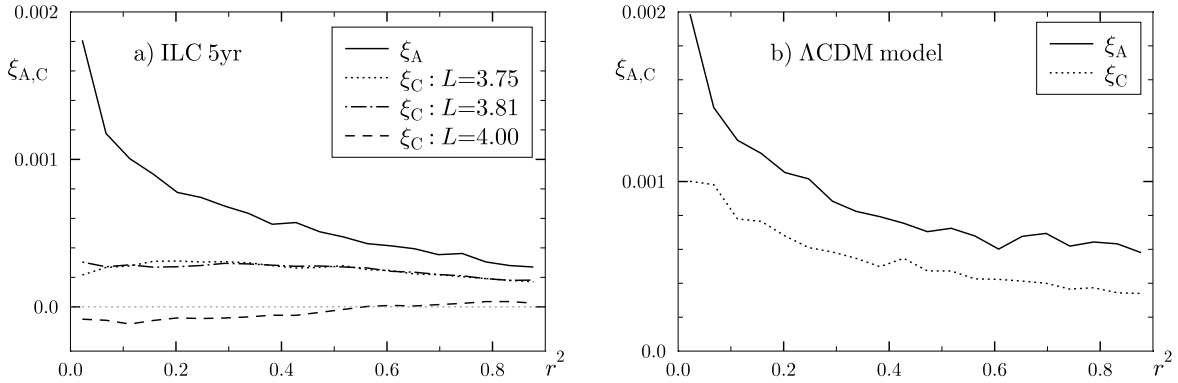


Figure 10. The cross-correlation ξ_C and the auto-correlation ξ_A are shown in panel a) for three toroidal cells: two with a correct orientation ($L = 3.75$ and $L = 3.81$) and one with a wrong size $L = 4.00$ and orientation ($\alpha = \beta = \gamma = 0$) using the 5yr ILC sky map. Panel b) displays ξ_C and ξ_A for the best toroidal cell for the "false positive" Λ CDM model. The kp0 mask is applied in all cases.

function signature are compatible with an equilateral toroidal structure. However, a firm conclusion cannot be drawn because of the high false positive rate.

In [1] the spatial-correlation-function method is applied to the Poincaré dodecahedral space and also a favoured orientation for this topology is found. Of course, only one of both topologies can be realized, if one of them at all. It is currently not clear which topology gives a better match to the data. In a following publication this question will be addressed by applying the spatial-correlation-function signature to several distinct topologies. Furthermore, it is intended to obtain a better estimate of the false positive rate.

Acknowledgments

OpenDX (www.opendx.org), CMBFAST (www.cmbfast.org) and HEALPix (healpix.jpl.nasa.gov) [15] as well as the WMAP data from the LAMBDA website (lambda.gsfc.nasa.gov) were used in this work.

References

- [1] B. F. Roukema, Z. Buliński, A. Szaniewska, and N. E. Gaudin, ArXiv e-prints **801** (2008), 0801.0006.
- [2] M. Lachièze-Rey and J. Luminet, Physics Report **254**, 135 (1995).
- [3] J. Levin, Physics Report **365**, 251 (2002).
- [4] J.-P. Luminet, ArXiv e-prints **802** (2008), 0802.2236.
- [5] N. J. Cornish, D. N. Spergel, and G. D. Starkman, Class. Quant. Grav. **15**, 2657 (1998).
- [6] G. Hinshaw *et al.*, Astrophys. J. Supp. **170**, 288 (2007), astro-ph/0603451.
- [7] G. Hinshaw *et al.*, ArXiv e-prints **803** (2008), 0803.0732.

- [8] N. J. Cornish, D. N. Spergel, G. D. Starkman, and E. Komatsu, *Phys. Rev. Lett.* **92**, 201302 (2004), astro-ph/0310233.
- [9] B. F. Roukema, B. Lew, M. Cechowska, A. Marecki, and S. Bajtlik, *Astron. & Astrophys.* **423**, 821 (2004), astro-ph/0402608.
- [10] R. Aurich, S. Lustig, and F. Steiner, *Mon. Not. R. Astron. Soc.* **369**, 240 (2006), astro-ph/0510847.
- [11] J. S. Key, N. J. Cornish, D. N. Spergel, and G. D. Starkman, *Phys. Rev. D* **75**, 084034 (2007), astro-ph/0604616.
- [12] B. S. Lew and B. F. Roukema, *ArXiv e-prints* **801** (2008), 0801.1358.
- [13] D. N. Spergel *et al.*, *Astrophys. J. Supp.* **170**, 377 (2007), arXiv:astro-ph/0603449.
- [14] N. Metropolis, A. W. Rosenbluth, M. N. Rosenbluth, A. H. Teller, and E. Teller, *J. Chem. Phys.* **21**, 1087 (1953).
- [15] K. M. Górski *et al.*, *Astrophys. J.* **622**, 759 (2005), HEALPix web-site: <http://healpix.jpl.nasa.gov/>.
- [16] J. Dunkley, M. Bucher, P. G. Ferreira, K. Moodley, and C. Skordis, *Mon. Not. R. Astron. Soc.* **356**, 925 (2005), arXiv:astro-ph/0405462.
- [17] R. Aurich, H. S. Janzer, S. Lustig, and F. Steiner, *ArXiv e-prints* **708** (2007), 0708.1420.